Biomaterials

Reporter cell activity within hydrogel constructs quantified from oxygen-independent bioluminescence

Dennis Lambrechts[a,c], Maarten Roeffaers[b], Greet Kerckhofs[a,c], Johan Hofkens[d], Tom Van de Putte[e], Jan Schrooten[a,c,*] , Hans Van Oosterwyck[c,f,*]

[a] Department of Materials Engineering, KU Leuven, Kasteelpark Arenberg 44 – box 2450, 3001 Leuven, Belgium.

[b] Center for Surface Chemistry and Catalysis, KU Leuven, Kasteelpark Arenberg 23, 3001 Leuven, Belgium.

[c] Prometheus, Division of Skeletal Tissue Engineering Leuven, KU Leuven, Herestraat 49 – box 813, 3000 Leuven, Belgium.

[d] Molecular Imaging and Photonics, KU Leuven, Celestijnenlaan 200F, 3001 Leuven, Belgium.

[e] TiGenix NV, Haasrode Researchpark 1724, Romeinse straat 12 box 2, 3001 Leuven, Belgium.

[f] Biomechanics Section, KU Leuven, Celestijnenlaan 300C – box 2419, 3001 Leuven, Belgium.

[*] To whom correspondence may be addressed.

E-mail: Hans.VanOosterwyck@kuleuven.be , Jan.Schrooten@kuleuven.be

Hans Van Oosterwyck, Celestijnenlaan 300C – box 2419, 3001, Leuven, Belgium

Jan Schrooten, Kasteelpark Arenberg 44 – box 2450, 3001 Leuven, Belgium

Keywords – Hydrogel, Bioluminescence, Spatial distribution, Model, Luciferase, Oxygen

Abstract

By providing a three-dimensional (3D) support to cells, hydrogels offer a more relevant *in vivo* tissue-like environment as compared to two-dimensional cell cultures. Hydrogels can be applied as screening platforms to investigate in 3D the role of biochemical and biophysical cues on cell behaviour using bioluminescent reporter cells. Gradients in oxygen concentration that result from the interplay between molecular transport and cell metabolism can however cause substantial variability in the observed bioluminescent reporter cell activity. To assess the influence of these oxygen gradients on the emitted bioluminescence for various hydrogel geometries, a combined experimental and modelling approach was implemented. We show that the applied model is able to predict oxygen gradient independent bioluminescent intensities which correlate better to the experimentally determined viable cell numbers, as compared to the experimentally measured bioluminescent intensities. By analysis of the bioluminescence reaction dynamics we obtained a quantitative description of cellular oxygen metabolism within the hydrogel, which was validated by direct measurements of oxygen concentration within the hydrogel. Bioluminescence peak intensities can therefore be used as a quantitative measurement of reporter cell activity within a hydrogel, but an unambiguous interpretation of these intensities requires a compensation for the influence of cell-induced oxygen gradients on the luciferase activity.

1. Introduction

Bioluminescence is the light that is generated through the enzyme-catalysed oxidation reaction of luciferase on its substrate, luciferin. This reaction enables the quantitative measurement of reporter cell activity via stable and sufficient integration of the luciferase reporter gene under control of a suitable promoter [1]. Most often the luciferase enzyme from the firefly, *Photinus pyralis*, is used as a reporter [2]. Activity of the firefly luciferase requires the presence of oxygen, ATP and Mg^{2+} to catalyse the conversion of luciferin into oxyluciferin accompanied by the release of a photon [3]. Although oxygen and ATP are frequently assumed to be readily present within the bioluminescent reporter cell assay, possible shortage in their supply may lead to an erroneous interpretation of the emitted bioluminescence intensities [4]. An approach in which possible shortages of these components can be quantified and that is able to compensate for their influence on the bioluminescence reaction, is therefore strongly required.

Various sources for the ambiguity in bioluminescent signal interpretation have already been identified and can for example be related to the positioning of the animal or sample [5], the direct effects of luciferase enzyme inhibitors (such as anaesthetics) or their indirect effects on the cardiovascular condition [6]. The latter effect would mainly influence the transport of luciferin to the reporter cells leading to a change in bioavailability of substrate for the bioluminescence reaction [4]. Not only the transport of luciferin via the blood has been suggested as possible mechanism for the modification in bioluminescence signal dynamics,

also changes in geometry of the multi-cellular tissue model [7] or the introduction of a hydrogel carrier [8] could strongly interfere with the observed dynamics.

Application of a hydrogel provides a 3D structural support for the cells which is more suitable for mimicking a physiologically relevant micro-environment to the cells [9, 10]. To create such a compatible environment, a multitude of different features (degradation, bioactivity, mechanical properties) can be engineered into the hydrogel [11]. Patterning approaches have thereby enabled independent integration and fine spatiotemporal control of these features *in situ*, such as the covalent photopatterning of thiol-containing functional groups within poly(ethylene glycol) (PEG) hydrogels that are produced via click chemistries [12]. Owing to the complexity of the 3D cell micro-environment and the numerous cues that exist, multifactorial methods are necessary to investigate these features and their combinations in high-throughput, e.g. by using robotic technology to simultaneously control type and concentration of spotted biomolecules and substrate stiffness [13, 14]. Hence hydrogels have been proposed as screening platforms to identify the instructive and regulatory mechanisms of various biochemical and biophysical cues on the fate of encapsulated cells [8, 15, 16]. Although their 3D micro-environment can be controlled through various modification and integration strategies, they come with some major design challenges that are associated with the adequate supply of oxygen and nutrients [17]. Unfortunately these limitations are also applicable to the availability of

luciferin substrate, therefore strongly complicating the analysis of the bioluminescent screening assay [18].

Motivated by the challenges of unambiguous bioluminescent signal interpretation and the significant variability that exists in performing bioluminescence measurements, several authors have explored the use of additional measurement parameters and assays to compensate for these effects. These measurements should then be performed in addition to the standard quantification of bioluminescence peak intensities. Among the reported analyses are the integrated signal intensities (or 'Area Under the Curve', AUC), peak times, parameters related to signal dynamics, and parallel orthogonal assays. Integrated intensities and AUCs have been identified as more suitable read-outs to match data obtained from anaesthetized with unanaesthetized conditions [6]. However, this parameter could not entirely compensate for the inhibitory effect on the luciferase activity, and in addition prolonged acquisition times would be required to obtain a value for this parameter. Peak times have been correlated with the size of multi-cellular spheroids [5]. Pharmacokinetic modelling approaches combined with bioluminescent signal dynamics has allowed for a better appreciation of the bio-distribution and availability of luciferin substrate within different cell culture systems [7, 19]. And finally, orthogonal assays have been proposed to assess specific interference of chemical compounds with luciferase reporter activity or to show reporter-independent activity [2, 20].

These strategies are better to deal with the variability in bioluminescent assays, but are based on the assumptions of a uniform presence and homogeneous distribution of reporter cells within the multicellular structure and the assumption of an easy accessibility to oxygen and luciferin. This study therefore aims at investigating the effects of cell spatial distribution (cells seeded uniformly or in monolayer configuration), hydrogel dimensions (diffusion distance), and cell-mediated oxygen gradients on the emitted bioluminescent light within an agarose hydrogel. We test the hypothesis that oxygen-independent bioluminescence intensities can be used as a quantitative measure of bioluminescent reporter cell activity within a hydrogel. Our strategy is based on the use of an experimentally validated mathematical model that we previously developed to describe the average photon flux emitted from bioluminescent reporter cells embedded within an agarose hydrogel [18]. We will further validate this model for the different hydrogel dimensions and seeding distributions. Finally, we will demonstrate how oxygen-independent, model-based bioluminescence intensities can be obtained that can be correlated to viable cell numbers.

2. Materials and Methods

2.1. 293T cell culture

Human embryonic kidney 293T cells were maintained in Dulbecco's modified Eagle's medium (DMEM) with Glutamax (Invitrogen, Merelbeke, Belgium) supplemented with 10% irradiated fetal bovine serum (Gibco), and 1% antibiotic-antimycotic (A/A) solution (100 units·ml^{-1} penicillin, 100 µg/ml streptomycin, and

0.25 µg/ml amphotericin B; Invitrogen). Cells were cultured at 37°C in a humidified atmosphere containing 5% CO_2. Medium was refreshed every 2-3 days and cells passaged when sub-confluent.

2.2. Cell transduction

293T cells were transduced with a lentiviral vector (pCH-EF1a-3flag-fLuc-T2A-eGFPIres-Bsd, 3.1 x 10^8 TU·ml^{-1}), which was a kind donation from Dr. Greetje Vande Velde (MoSAIC, KU Leuven). The day before transduction, cells were seeded in a 96-well plate at 1 x 10^4 cells per well. On the day of transduction, medium was replaced by DMEM containing serial dilutions of the vector and incubated for 24 hours. After 24 hours, medium was replaced with DMEM containing 1 µg·ml^{-1} blastidicin for antibiotic selection of the stably transduced cell population, and was continued for 2-3 weeks. Transduction efficiencies were analyzed by flow cytometric analysis (FACS).

2.3. Hydrogel screening setup

Low melting point agarose hydrogels (2% in DMEM, Invitrogen) containing stably transduced 293T cells were prepared in wells of a 96 well black plate (MicroWell 96-well optical-bottom plates, Nunc, Thermo Scientific). Cells were either uniformly distributed within the hydrogel or contained as a monolayer underneath the hydrogel (Fig. 1). Three different hydrogel heights (2 mm, 4 mm, and 6 mm) were prepared for both monolayer and uniformly seeded conditions. Cell were seeded at a density of 1 x 10^6 cells·ml^{-1} for the uniform distribution, which

resulted in a total cell number of 6.4 x 10^4 (2 mm), 12.8 x 10^4 (4 mm), and 19.2 x 10^4 (6 mm). Total cell numbers and seeding densities were equal for the monolayer distribution, which resulted in cell surface densities of 2, 4, and 6 x 10^5 cell·cm^{-1}, respectively. For the monolayer configuration, cells were seeded in cell culture surface coated wells and allowed for cell attachment during a 3 hour period. After this period the hydrogel was poured into the well and gelation was continued for 5 min. Upon completion of the gelation process, a total amount of 100 µl DMEM was transferred to the wells and the well plate was incubated at 37°C in a humidified atmosphere containing 5% CO_2.

2.4. Oxygen measurements

Measurements of oxygen concentration were performed with sensor spots (PSt3, PreSens, Regensburg, Germany) mounted to the coverglass bottom of the optical well plate. Signals obtained from the sensor spot were transmitted via a polymer optical fiber to a fiber optic oxygen transmitter (Fibox 3, PreSens, Regensburg, Germany). The sensor spots were calibrated in the wells by two-point calibration with oxygen-saturated DMEM and oxygen-free DMEM (1% Na_2SO_3 in DMEM), according to the manufacturer's instructions. After calibration, cells and hydrogel were introduced into the well as described before. Oxygen measurements were performed before and after every dynamic bioluminescence reporter assay.

2.5. Fluorescence Recovery after Photobleaching (FRAP)

Low melting point agarose gels (Invitrogen) with a final concentration of 2% were prepared. Gels were incubated with DMEM containing a 25 μM concentration of fluorescein (Sigma). After overnight incubation, slides and gels were transferred to the stage of a confocal fluorescence microscope (FluoView 1000, Olympus) equipped with a UPLSAPO 10x air objective (NA: 0.40) used for observation. Measurements were performed at 37°C. Fluorescence images were collected with the systems PMT. A 488 nm Ar laser was used to bleach and also monitor the recovery of fluorescein tracer molecules. The pinhole size was set to 50 μm. Images were acquired with 72 ms intervals during a 3 s scanning period, and consisted of 256 x 256 pixels with a pixel size of 0.497 x 0.497 μm (zoom factor: 10). Prebleaching images were acquired to compensate for nonuniform light illumination. Circular regions (radius, 10 μm) were bleached (total bleaching time, 13 ms) with the laser in tornado-scan mode (SIM Scanner, Olympus). Image analysis was performed with a program written in MATLAB (The MathWorks, Natick, MA). The method implemented into this program is based on a spatial frequency analysis of circularly averaged radial intensities of each image [21]. In brief, the recovery of fluorescent tracer was modeled according to Fick's second law. An analytical solution to this equation was obtained via the Hankel transform. Circular averaging on the radial intensities was performed to reduce the noise in the intensity profiles. Finally the analytical solution was fitted to the experimental curves using a nonlinear curve fitting algorithm in MATLAB. We also verified the independence of diffusion rates on spatial frequency, as our setup is characterized by Brownian diffusion. Analysis was performed for a single

diffusing component with the fraction of immobile molecules set to zero. Spatial heterogeneities in tracer diffusivity were detected by FRAP imaging at different circumferential positions along 3 radial positions in the gel (imaging depth, 150 µm). Measurements were performed in duplicate on each gel with a small shift in spatial position.

2.6. Single-cell bioluminescence microscopy

Glass coverslides were coated with 500 µl Poly-L-Lysine (PLL, Sigma) solution (0.1%, 5 min), rinsed with Milli-Q water, and dried overnight. 1 x 10^5 293T cells were plated on PLL-coated coverslips. After overnight cell attachment, these slides were placed on the stage of a luminescence microscope (LuminoView 200, Olympus). Cells were incubated with a 4.7 µM luciferin solution in DMEM at 37°C (Solent Scientific). Bioluminescence was imaged with an UPLSAPO 60x silicon oil objective (NA: 1.3) and transmitted to a cooled CCD camera (ImagEM512, Hamamatsu Photonics) mounted on the bottom port of the microscope. Time-lapse images were collected with 30 s acquisition times and EM gain was set at 1200x (photon imaging mode, Hamamatsu). Regions of interest were defined around the cell contours from which the average bioluminescence intensities were calculated.

2.7. Bioluminescence intensity measurements from cell seeded hydrogels

Culture medium located on top of the hydrogels (Fig. 1) was replaced with DMEM supplemented with 4.7 µM luciferin (Promega). The screening setup was then

transferred to the stage of an *in vivo* imaging system (IVIS 100, Perkin-Elmer, USA). Images were taken with a 1-inch CCD camera cooled to -105°C. The field of view (FOV) was set to 10 x 10 cm. Image sequences (acquisition time, 2 min) were acquired with 5 min intervals during a scanning period of 3 hours, followed by 10 min intervals during a 7 hour period. Images were processed in the LivingImage software (Perkin-Elmer) and radiance units refer to the number of photons per second that are leaving a square centimetre of the hydrogel and are radiating into a solid angle of one steradian (Ω, fraction of the isotropic radiation field, which can be thought of as a three-dimensional cone of light emitted from the surface). All measurements were performed at 37°C.

2.8. Quantification of viable cell numbers in agarose hydrogels

Viable cell numbers were quantified using the Live/Dead viability/cytotoxicity kit (Invitrogen). Agarose constructs were rinsed with PBS solution, covered with Live/Dead staining solution containing 2 μM calcein AM and 4 μM ethidium homodimer-1 in PBS, and incubated for 1 hour in the dark. The dye solution was discarded afterwards and background due to residual stain was washed away with PBS. Image stacks were obtained on a confocal laser scanning microscope (CLSM, Fluoview 1000, Olympus) equipped with an UPLSAPO 10x air objective (NA: 0.4). Images were acquired with a pixel size of 2 x 2 μm and a nominal z step size of 20 μm to a depth of about 250 μm within the hydrogel. Live and dead cell numbers were counted via a sphere fitting algorithm in Imaris Bitplane (Zurich, Switzerland). DNA content was evaluated according to a protocol

described by Grayson et al. [22]. Briefly, agarose constructs were washed in PBS, transferred to 400 µl of digestion buffer (10 mM Tris, 1 mM EDTA, and 0.1% Triton X- 100) with 0.1 mg/ml proteinase K in centrifugation tubes, and incubated at 56°C for 3 hours. Supernatant was collected after removal of debris by centrifugation (13,000 rpm, 1 min) and measured with a Qubit system (Invitrogen).

2.9. Correlation analysis

Correlations of simulated and experimentally measured bioluminescence data sets were calculated using the Pearson's correlation coefficient. Correlation coefficients were also determined for oxygen-dependent and oxygen-independent bioluminescence data sets with the viable cell densities (Table 2). Calculations were performed in MATLAB using the corr2 MATLAB function.

3. Mathematical model

3.1. Model geometry

Due to the impermeable lateral walls and constant cross-sectional geometry of the hydrogel screening setup (Fig. 1), molecular transport can only take place in the vertical direction. As such, transport equations only have time and the vertical coordinate as independent variables and a one-dimensional domain can be defined along the vertical dimension of the setup. Within this domain, two regions were identified for hydrogels that were uniformly seeded with reporter cells (namely hydrogel and culture medium) and three regions for hydrogels that

contained reporter cells in a monolayer configuration (cell layer, hydrogel, and culture medium). Simulations were performed for three different hydrogel heights of 2 mm, 4 mm, and 6 mm.

3.2. Model equations

The mathematical model that was used in this study is based on a previously developed model to describe the average photon flux emitted from bioluminescent reporter cells embedded within an agarose hydrogel [18]. This model contains a set of five partial differential equations that mathematically describe the spatiotemporal changes in oxygen availability (c_{O_2}), luciferin concentration (c_{Dluc}), intracellular luciferase concentration (c_{luc}) and bioluminescent light generation (c_L). Most model parameters were obtained from the previous study, except for the luciferin uptake (k_{cat} and $D_{luc,m}$) and decay kinetics (I_{21}), which were changed to account for the lower luciferin concentration used in this study. These parameter changes are also indicated in Table 1.

Variations in intra- and extracellular luciferin concentrations were decoupled and implemented into the model as two separate variables ($c_{Dluc,I}$ and $c_{Dluc,E}$, respectively) and equations that account for their change. Extracellular luciferin concentration changed as a result of diffusion (described by Fick's second law, with the luciferin diffusion coefficient, $D_{Dluc,E}$), active uptake by the cells (membrane diffusion coefficient, $D_{Dluc,m}$), and natural decay of the substrate (lucferin decay rate, $k_{d,Dluc}$).

$$\frac{\partial c_{Dluc,E}(z,t)}{\partial t} = D_{Dluc,E}(z,t) \cdot \frac{\partial^2 c_{Dluc,E}(z,t)}{\partial z^2} - \frac{D_{Dluc_m} A_m}{\lambda_m} \cdot$$

$$\left(c_{Dluc,E}(z,t) - c_{Dluc,I}(z,t)\right) \cdot c_{cell}(z,t) - k_{d,Dluc} \cdot c_{Dluc,E}(z,t) \quad (1)$$

In this equation A_m is the membrane surface area of a reporter cell, λ_m is the thickness of the cell membrane, and $k_{d,Dluc}$ is the luciferin decay constant. Luciferin substrate molecules taken up by the cells are enzymatically converted into oxyluciferin, in a bioluminescence reaction process that is accompanied by the emission of a photon. Luciferin conversion rates are dependent on the available luciferin substrate concentration and can be described by a Michaelis-Menten law. Time-dependent decay of bioluminescent light emission was described by a first order kinetic equation [23]. The straightforward implementation of this equation with a single decay parameter has a clear advantage in describing reactions that undergo exponential decay [24].

$$\frac{\partial c_{Dluc,I}(z,t)}{\partial t} = \frac{D_{Dluc_m} A_m}{\lambda_m} \cdot \left(c_{Dluc,E}(z,t) - c_{Dluc,I}(z,t)\right) \cdot c_{cell}(z,t) - k_{d,Dluc} \cdot$$

$$c_{Dluc,I}(z,t) - k_{cat}\left(c_{O_2}\right) \cdot e^{\sigma(t-t_i(z,t))} \cdot \frac{c_{Dluc,I}(z,t)}{K_m(c_{O_2}) \cdot \Gamma + c_{Dluc,I}(z,t)} \cdot c_{luc} \quad (2)$$

$$\frac{\partial c_L(z,t)}{\partial t} = k_{cat}\left(c_{O_2}\right) \cdot e^{\sigma(t-t_i(z,t))} \cdot \frac{c_{Dluc,I}(z,t)}{K_m(c_{O_2}) \cdot \Gamma + c_{Dluc,I}(z,t)} \cdot c_{luc} \cdot RLU \quad (3)$$

In this equation c_{cell} is the cell density, k_{cat} is the catalytic rate constant, K_m is the Michaelis Menten constant, σ is the exponential decay constant, and RLU is a light conversion factor. Gradients in available oxygen concentration originated from a balance in oxygen consumption rates from the cells (OCR, Q_{O_2}) and oxygen diffusion rates through the gel (oxygen diffusion coefficient, D_{O_2}).

$$\frac{\partial c_{O_2}(z,t)}{\partial t} = D_{O_2}(z,t) \cdot \nabla^2 c_{O_2}(z,t) - Q_{O_2}(z,t) \cdot c_{cell}(z,t) \quad (4)$$

In this equation OCRs were also described by a Michaelis-Menten kinetic equation.

$$Q_{O_2}(z,t) = Q_{max}\frac{c_{O_2}(z,t)}{K_{m,O_2}+c_{O_2}(z,t)} \quad (5)$$

Intracellular firefly luciferase concentrations (c_{luc}) remained constant during cell culture as their expression was under control of a constitutive promoter. Changes in average luciferase concentration contained within the construct resulted from corresponding changes in cell density.

These coupled partial differential equations were solved numerically using a previously developed finite volume code. The grid size was 100 µm. We used the ROWMAP code for time integration of the numerical algorithm [25].

3.3. Intracellular luciferin uptake

We implemented a diffusion model that was shown to be successful in describing long-term (hours) luciferase activity in living cells [19]. Estimations for the cellular luciferin influx were obtained from fitting a membrane diffusion model through the short term dynamic time point measurements of luciferase activity in intact cells (Fig. 3A). This resulted in a value of 1.4 x 10^{-11} $m^2 \cdot s^{-1}$ for the luciferin transmembrane diffusion coefficient ($D_{luc,m}$ in equations 1 and 2) for an exogenous luciferin concentration of 4.7 µM.

3.4. Bioluminescent light generation

The intracellular conversion of luciferin into oxyluciferin followed a Michaelis-Menten kinetics that we modified to describe the influence of available oxygen

concentration. Kinetic parameters were quantified under normoxic and hypoxic conditions [18]. Parametric changes for intermediate oxygen concentrations were reasoned to follow a square root dependent relationship, similar to ATP [26], another cofactor of the bioluminescence reaction.

3.5. Decay initialization time

Exponential decay of bioluminescent light emission was described by a first order kinetic equation. The spatial distribution of reporter cells contained within the hydrogel, combined with developed gradients in available luciferin concentration, mandated the introduction of a time initialization parameter (t_i). This parameter was used to accurately describe time- and space-dependent occurrence of bioluminescence reactions and their subsequent activity decay. The criterion for re-initialization of the cytoplasmic bioluminescence reaction was made dependent on the magnitude of intracellular luciferin influx.

$$t_0^{i+1} = t_0^i + (t - t_0^i) \cdot \frac{\kappa(c_{O_2}) \cdot {c^{i+1}}_{Dluc,I}(z,r,t) - {c^i}_{Dluc,I}(z,r,t)}{\kappa(c_{O_2}) \cdot {c^{i+1}}_{Dluc,I}(z,r,t)} \quad \text{for} \quad {c^{i+1}}_{Dluc,I}(z,r,t) > {c^i}_{Dluc,I}(z,r,t)$$

$$t_0^{i+1} = t_0^i \quad \text{for} \quad {c^{i+1}}_{Dluc,I}(z,r,t) \leq {c^i}_{Dluc,I}(z,r,t) \tag{6}$$

3.6. Initial and boundary conditions

Viable cell densities were assumed to remain constant during the dynamic reporter cell assay (10 hour experiment) and were obtained for each culture day from the DNA and viability assays outlined in the Materials and Methods section. For the uniformly cell seeded hydrogels, a homogeneous distribution of cell

density and viability within the hydrogel was implemented for the entire culture time. Luciferin substrate was added to the culture medium after 12 h (day 1), 36 h (day 2), 60 h (day 3) culture periods. Concentrations were assumed to be homogeneously distributed in the medium. This condition was ensured by initial mixing of the medium at the luciferin bolus time. Initial oxygen concentrations were set to 0.192 $mol \cdot m^{-3}$ (oxygen solubility in water at 37°C) or 21%. Mixing during the luciferin bolus time also resulted in a redistribution of available oxygen concentrations, which we implemented by resetting the oxygen concentration (initial condition) in the culture medium to 21%.

The mathematical model was closed by insertion of suitable boundary conditions. No-flux boundary conditions were applied for all boundaries, except for the top surface of the culture medium where a Dirichlet boundary condition was applied of 21% oxygen concentration during the total experiment duration.

4. Results

Quantitative and non-invasive measurements of luciferin diffusion rates within the cell-seeded hydrogels were obtained from fluorescence recovery after photobleaching (FRAP), using fluorescein as a suitable fluorescent tracer analogue. FRAP measurements indicated no significant changes in tracer diffusivity with culture time and revealed an average value of 260 $\mu m^2 \cdot s^{-1}$ (Fig. 2).

The model accounts for the oxygen-dependent firefly luciferase activity by changing bioluminescent photon fluxes, initial reaction kinetics, and decay rates

according to the oxygen conditions to which cells are exposed. As discrepancies in bioluminescence signal dynamics were previously observed between the model simulations (for model parameter values established in [18]) and experimental measurements for cells exposed to lower luciferin concentrations, we quantified the effect of a lower luciferin concentration on the bioluminescence decay rate. Data obtained from single cell bioluminescence microscopy was therefore fitted to our modelling results (Fig. 3). This fitting procedure resulted in changes in parameter values for decay rate (I_{21}), catalytic rate constant (k_{cat}), and active luciferin membrane transport ($D_{luc,m}$) for reporter cells incubated with 4.7 μM luciferin and exposed to normoxic conditions. Other model parameter values were used as determined in [18] and are summarized within Table 1.

Dynamic time point measurements of the average photon flux were obtained for three different hydrogel dimensions (2, 4, and 6 mm hydrogel thickness). This data was fitted with the updated model, using the cell oxygen consumption rate (OCR, Q_{max} in equation (5)) as the only fitting parameter (Fig. 4). Both the simulated and the experimentally obtained bioluminescence data sets contained peak intensities that occurred faster for the hydrogels with a uniform cell distribution (peak occurrence within 2 hours) as compared to the monolayer distribution (several hours). Correlation analysis of the fitted model and the experimental data is shown in Figure 4G. This analysis generally revealed a stronger correlation for the initial time points (2 hours period) as compared to the total duration of the experiment (10 hours period). Only for the monolayer seeded

hydrogels of 4 and 6 mm thickness, a strongly decreased correlation was observed for the initial time points. Quantification of the averaged bioluminescence peak intensities showed that simulated peak intensities nicely corresponded to the experimentally measured values (Fig. 5, 6). OCR values that were determined from curve fitting generally abated with culture time and were characterized by an average value (Q_{max} in equation 5) of 1.5 x 10^{-17} mol·cell^{-1}·s^{-1}, for cells embedded as a monolayer underneath the hydrogel, and 2.32 x 10^{-17} mol·cell^{-1}·s^{-1}, for reporter cells that were uniformly distributed within the hydrogel. Using these OCR values, we were able to predict oxygen gradients that were induced inside the hydrogel constructs (Fig. 7). Predicted oxygen values at the hydrogel bottom surface were validated by comparison with the oxygen measurements obtained from oxygen sensor spots that were integrated below the hydrogel. Experimental measurements yielded an anoxic read-out (0% O_2 for sensor spots calibrated in 1% Na_2SO_3) at the bottom position for each configuration and for every hydrogel thickness. This was also found for all model simulations, apart from the simulations for the 2 and 3 days culture of a uniform cell distribution in the thickest hydrogel (6 mm). For these conditions, the lowest available oxygen concentrations that would be present at the hydrogel bottom position were predicted to be 5.9% and 12%, respectively.

Finally, we explored the use of our approach to resolve the influence of oxygen gradients on the luciferase activity and assessed its application for making quantitative measurements of bioluminescence signals emitted from luciferase

reporter cells encapsulated within a hydrogel. For each hydrogel setup an oxygen gradient-free condition was simulated, by imposing a uniform and saturated (21%) oxygen concentration throughout the hydrogel. Model simulations that were obtained in this way therefore represent the oxygen-independent bioluminescence signal intensities. These intensities are based on signal dynamics that are solely influenced by the hydrogel thickness (geometrical feature) and the cell seeding pattern (homogenous or monolayer distribution), and therefore represent a robust measure of the active reporter cell population (Fig. 8). As such, the predicted peak intensities retrieved from the oxygen-independent bioluminescent signal simulations were able to better capture the observed trends in viable cell numbers (Fig. 5, 6, 8). Analogies in simulated, oxygen-independent peak intensities and measured viable cell numbers were confirmed by correlation analysis, for which correlation coefficients near unity were obtained for both homogenously and monolayer-seeded hydrogels, in contrast to the generally (much) lower or even negative correlation coefficients between measured (and therefore oxygen-dependent) bioluminescence peak intensities and viable cell numbers (Table 2). These results are further clarified by the relative differences shown in figure 9. The strongest deviations in correspondence between measured bioluminescence peak intensities and viable cell numbers were observed for the thickest hydrogels (6 mm) and for the 2 mm thick hydrogels containing a cell monolayer. Measurement correspondence for the uniformly seeded hydrogels decreased with increasing hydrogel thickness. This observation coincided with an increasing amount of reporter cells that is

exposed to different oxygen concentrations (i.e. extent of oxygen gradient in Fig. 7A-C), and therefore stresses the importance to compensate for cell-mediated influences of oxygen tension on the emitted bioluminescence signal.

4. Discussion

Bioluminescent light emitted from multi-cellular reporter systems suffers from a strong variability in quantified signal intensities [4, 5, 7]. The presence of cell-induced oxygen gradients has been identified as a potential source for this variability [18]. Possible differences in oxygen gradients can be induced by altered cell-biomaterial interactions [27], cell spatial distributions and cell densities [17, 28], or as a result of chemical agents acting on cell metabolism [29, 30]. Guaccio et al. previously reported a ~2 fold change in OCR for bovine chondrocytes seeded in collagen as compared to agarose hydrogels [27]. As strong oxygen gradients can be established both *in vitro* as well as *in vivo* [17, 31, 32], an approach is required to compensate for the influence of these gradients on the measured bioluminescence intensities and to enable an unambiguous interpretation of bioluminescent reporter cell activity.

The approach that we implemented for the hydrogel screening setup presented here, is based on a combined experimental and computational study in which oxygen-independent bioluminescence intensities are obtained from a previously developed and experimentally validated mathematical model [18]. Relevant model parameters and geometry were updated to account for the hydrogel setup

used in this study (Table 1). Dynamic time point measurements of the average bioluminescent photon flux were fitted with the updated model. Keeping the oxygen diffusion coefficient through the agarose hydrogel constant with culture time - which can be justified based on the constant fluorescein diffusion coefficient as measured by FRAP (Fig. 2) - we could use cellular OCR as the only fitting parameter.

Generally, a better correspondence between experimental and simulated bioluminescence data sets was observed for the initial (2 hours) time points as compared to the total experiment duration (10 hours). The monolayer seeded hydrogels of 4 and 6 mm thickness had a high standard deviation for the initial time points of the experimentally measured bioluminescence signals. This variability interfered with the analysis results and therefore resulted in a decrease in correlation coefficient. By comparison to the peak positions of the 2 mm thick hydrogels, peak intensities of the thicker 4 and 6 mm hydrogels can be expected to occur after the initial 2 hours period due to the increase in diffusion distance. Significantly higher correlation was observed for the longer time periods, therefore justifying further analysis.

Values for OCR obtained from model fitting are in good agreement with previously reported OCR values for mesenchymal stem cells seeded in agarose ([33], 1.35 x 10^{-17} mol·cell^{-1}·s^{-1}), and OCR of 293T cells cultured in monolayer configuration ([34], 3.3 x 10^{-17} mol·cell^{-1}·s^{-1}). Peak values in OCR data were

observed after 1 day of culture for the homogeneously cell seeded hydrogels of 2 mm and 6 mm thickness (Fig 5D). Interestingly, these changes corresponded to a strong increase in viable cell numbers from day 1 to day 2, with ~3 fold for the 2 mm thick hydrogel and ~1.5 fold for the 6 mm thick hydrogel (fig. 5A,C). Average predicted OCRs for 293T cells seeded in monolayer underneath the hydrogel (1.5×10^{-17} mol·cell^{-1}·s^{-1}) were lower than for 293T cells uniformly distributed within the hydrogel (2.32×10^{-17} mol·cell^{-1}·s^{-1}) (Fig. 5D, Fig. 6D). This observation is in line with previous studies reporting that oxygen consumption by the cells is decreased when cells are exposed to a decreased oxygen concentration [35] (Fig. 7). Predicted oxygen concentrations at the bottom of the hydrogel were validated by comparison to oxygen read-outs obtained from an oxygen patch sensor. Anoxic read-outs were obtained at the bottom position for every hydrogel thickness and for both seeding distributions, which was in agreement with the model simulations, apart from the simulations of the 2 and 3 days culture of the uniform cell distribution in the thickest hydrogel (6 mm).

For the current model, we were most interested in the bioluminescence peak intensities, as these peaks are used most often as a quantitative read-out for reporter cell activity [8, 36]. Oxygen-dependent simulated and experimentally measured peak intensities were in good agreement (Fig. 5, 6), but were generally unable to capture the observed changes in viable cell densities. This divergent behaviour confirms the need to compensate for the influence of oxygen gradients on the bioluminescence intensities. Correlation analysis revealed a higher

correspondence between the viable cell densities and the predicted peak intensities retrieved from the oxygen-independent bioluminescent signal simulations (correlation coefficients near unity, Table 2). This illustrates the main strength of our modelling approach, which lies in its ability to easily resolve the influence of oxygen gradients on the luciferase activity.

In practice, both the OCR and viable cell densities are unknown parameters that need to be determined from the bioluminescence fitting algorithm. Changes in these parameter values result in different oxygen distributions, according to the relation described by equation (4). Necessary information on the oxygen distribution can be obtained from non-anoxic measurements using oxygen sensor spots, that are positioned at the hydrogel bottom location, or from oxygen measurements using oxygen sensitive microbeads (OSB) contained within the hydrogel [18]. Assuming a constant oxygen diffusion rate and a homogeneous cell distribution within the hydrogel, the OCR and viable cell number will be inversely related when trying to fit a given (i.e. experimentally determined) oxygen distribution, according to equation (4) (solved for the steady state). With other words, for a given steady-state oxygen distribution, the OCR needs to be decreased when more viable cells are assumed to be present within the hydrogel, and vice versa. This condition, implied by equation (4), should therefore be satisfied when the oxygen-dependent simulated and experimentally quantified bioluminescence data sets are fitted.

As the hydrogel constructs were incubated with a lower (4.7 μM) luciferin concentration than the concentration used for establishment of the mathematical model (470 μM) [18] and because we previously observed discrepancies in bioluminescence signal dynamics between the model simulations and experimental measurements for cells exposed to lower luciferin concentrations, some modifications in parameter values for the luciferin uptake (k_{cat} and $D_{luc,m}$) and decay kinetics (I_{21}) were performed. First of all, luciferin is required as a substrate for the membrane-bound ABC transporters that control the net influx of luciferin into the cytoplasm [37, 38]. Lowering the available luciferin concentration would therefore result in a decreased uptake rate. This was also reflected in the updated model by a decrease in the membrane transport coefficient for luciferin ($D_{luc,m}$ is 1.4 x 10^{-11} $m^2 \cdot s^{-1}$) as compared to the previous model (8 x 10^{-11} $m^2 \cdot s^{-1}$) [18]. Furthermore, the decrease in active uptake and lowered availability of intracellular luciferin molecules could induce shifts in the ratiometric balance between the luciferin and its reaction stabilizing components, therefore leading to a slower decay rate [39-41]. A decay rate (I_{21}) of 2.5 s^{-1} was implemented in the updated model, which was slower than the 27 s^{-1} decay rate which we used previously [18]. One of these components involved in bioluminescence decay dynamics is the inorganic pyrophosphate concentration (PPi). PPi can bind to firefly luciferase, preventing the formation of the catalytically inactive dehydroluciferyl-adenylate (L-AMP) complex [39], which has been identified as an important pathway responsible for the bioluminescence decay [42-44]. As PPi is a product of the luciferase reaction, higher luciferin concentrations would lead

to higher PPi levels and therefore a reduced decay rate. However, increased PPi concentrations also have an inhibitory effect on the luciferase activity, by preventing the ATP-binding and hence increasing the bioluminescence decay rates that can be observed [39]. Binding of PPi to the luciferase enzyme can consequently disturb the balance between stabilization and inactivation of the bioluminescence reaction. Another component influencing the decay dynamics is Coenzyme A (CoA) [40-42, 45]. CoA can stabilize the photon production by thiolysis of L-AMP into dehydroluciferyl-coenzyme A (L-CoA), which is a less powerful inhibitor than L-AMP on the bioluminescence reaction [40]. Direct influences of both components, PPi and CoA, were however not implemented into the model.

Bioluminescence decay rates were measured for intact 293T cells using a bioluminescence microscopy setup (LV 200, Olympus). This setup enabled the acquisition of bioluminescent light emitted from reporter cells that were maintained in a focused position. As indicated earlier, application of a lower luciferin concentration (4.7 µM) resulted in a slower luciferin uptake rate, as compared to the value implemented in our previous model [18], which was evidenced by the diminished slope of initial luciferase activity and an increased time to peak activity of about 16 min (Fig. 3). Decay rate (I_{21}) was also reduced at this luciferin concentration and the bi-exponential decay that we observed previously [18], was almost completely absent. Alterations in decay rate and luciferin uptake rate were subsequently implemented into the model, and

changes in catalytic rate constant (k_{cat}) were allowed to obtain equal peak bioluminescence intensities between the previous model and the updated model. This procedure was followed for reporter cells exposed to normoxic conditions. At anoxic conditions, cells detached and could consequently no longer be visualized in a focused position. The same model parameters for decay rate (I_0) and catalytic rate constant ($k_{cat,0}$) were therefore chosen as experimentally quantified in our previous study [18]. This approach could be justified by the observation that the stabilizing effect of CoA on the bioluminescence reaction is more pronounced for higher concentrations of ATP [40], and consequently also at increased levels of oxygen availability to the cells [18, 35, 46].

The thickest hydrogels (6 mm) uniformly seeded with bioluminescent reporter cells showed a discrepancy between predicted and experimentally measured oxygen concentrations, induced after 2 and 3 days of static culture. This observation could possibly be attributed to the more substantial contribution of reporter cells located at the peripheral top position to the emitted bioluminescence signal, as compared to cells located at the bottom region of the hydrogel. Decreased accessibility to luciferin and oxygen could thereby explain the reduced photon fluxes that are emitted from reporter cells located at the hydrogel bottom, which can complicate further analysis or result in erroneous conclusions. These are important limitations that depend on the applied reporter substrate concentration, and should therefore be taken into consideration in the design of a setup for hydrogel screening.

In addition to the differences in substrate availability, cells located at the hydrogel peripheral top position possibly also contain other mechanisms to further stabilize the bioluminescence reaction that were not accounted for in our model. Such a mechanism could have contributed to the predicted overestimation of available oxygen concentration, but could also explain the differences in fitting longer time point dynamics (Fig. 4). For example, the post-translational targeting and compartmentalization of firefly luciferase to peroxisomes could potentially interfere with degradation kinetics of the enzyme, thereby influencing the emitted photon flux [47-49]. Therefore, if fitting of longer bioluminescence reaction dynamics would be required, additional stabilization equations would need to be introduced into the current model. This model would then be extremely valuable for the quantitative determination of time periods in which hydrogel screening experiments should be performed. But its applicability would also extend to the optimization of experimental protocols for repeated bioluminescence measurements. Since residual luciferin could potentially interfere with these measurements, the model would be an important tool in optimizing the rinsing procedures.

5. Conclusions

In this study we applied a combined experimental and modelling approach to describe the average photon flux emitted from bioluminescent reporter cells embedded within a hydrogel screening setup. Using this approach, we were able

to obtain quantitative information on cell oxygen metabolism within the hydrogel. Furthermore, it was shown that peak intensities can be used as a quantitative measure of bioluminescent reporter cell activity, but that an unambiguous interpretation of these intensities requires a model-based compensation for the influence of cell-mediated oxygen gradients on the luciferase activity.

Acknowledgements

This work was supported by the agency for Innovation by Science and Technology (IWT-Vlaanderen, project number 090727) and the Research Foundation-Flanders (FWO-Vlaanderen, project number G.0858.12). The authors also gratefully acknowledge financial support from the Flemish Government through long-term structural funding ‘‘Methusalem’’ (CASAS Methusalem grant) and from the Hercules Foundation (HER/08/021). Usage of the IVIS100 system was funded by a MoSAIC internal project (www.saic.be). We acknowledge the Olympus Corporation for providing the LV200 on loan. This work is part of Prometheus, the Leuven Research & Development Division of Skeletal Tissue Engineering of the KU Leuven (www.kuleuven.be/prometheus).

References

[1] Prescher JA, Contag CH. Guided by the light: visualizing biomolecular processes in living animals with bioluminescence. Curr Opin Chem Biol. 2010;14:80-9.

[2] Thorne N, Inglese J, Auld DS. Illuminating insights into firefly luciferase and other bioluminescent reporters used in chemical biology. Chem Biol. 2010;17:646-57.

[3] Roda A, Guardigli M, Michelini E, Mirasoli M. Bioluminescence in analytical chemistry and in vivo imaging. Trends Anal Chem. 2009;28:307-22.

[4] Keyaerts M, Caveliers V, Lahoutte T. Bioluminescence imaging: looking beyond the light. Trends Mol Med. 2012;18:164-72.

[5] Cui K, Xu X, Zhao H, Wong ST. A quantitative study of factors affecting in vivo bioluminescence imaging. Luminescence. 2008;23:292-5.

[6] Keyaerts M, Remory I, Caveliers V, Breckpot K, Bos TJ, Poelaert J*, et al.* Inhibition of firefly luciferase by general anesthetics: effect on in vitro and in vivo bioluminescence imaging. PLoS One. 2012;7:e30061.

[7] Sim H, Bibee K, Wickline S, Sept D. Pharmacokinetic modeling of tumor bioluminescence implicates efflux, and not influx, as the bigger hurdle in cancer drug therapy. Cancer Res. 2011;71:686-92.

[8] Weiss MS, Bernabe BP, Bellis AD, Broadbelt LJ, Jeruss JS, Shea LD. Dynamic, large-scale profiling of transcription factor activity from live cells in 3D culture. PLoS One. 2010;5:e14026.

[9] Gilbert PM, Blau HM. Engineering a stem cell house into a home. Stem Cell Res Ther. 2011;2:1-9.

[10] Bencherif SA, Sands RW, Bhatta D, Arany P, Verbeke CS, Edwards DA*, et al.* Injectable preformed scaffolds with shape-memory properties. Proc Natl Acad Sci U S A. 2012;109:19590-5.

[11] Seliktar D. Designing cell-compatible hydrogels for biomedical applications. Science. 2012;336:1124-8.

[12] DeForest CA, Polizzotti BD, Anseth KS. Sequential click reactions for synthesizing and patterning three-dimensional cell microenvironments. Nat Mater. 2009;8:659-64.

[13] Lutolf MP, Gilbert PM, Blau HM. Designing materials to direct stem-cell fate. Nature. 2009;462:433-41.

[14] Gobaa S, Hoehnel S, Roccio M, Negro A, Kobel S, Lutolf MP. Artificial niche microarrays for probing single stem cell fate in high throughput. Nat Methods. 2011;8:949-55.

[15] Chatterjee K, Lin-Gibson S, Wallace WE, Parekh SH, Lee YJ, Cicerone MT*, et al.* The effect of 3D hydrogel scaffold modulus on osteoblast differentiation and mineralization revealed by combinatorial screening. Biomaterials. 2010;31:5051-62.

[16] Benoit DS, Schwartz MP, Durney AR, Anseth KS. Small functional groups for controlled differentiation of hydrogel-encapsulated human mesenchymal stem cells. Nat Mater. 2008;7:816-23.

[17] Demol J, Lambrechts D, Geris L, Schrooten J, Van Oosterwyck H. Towards a quantitative understanding of oxygen tension and cell density evolution in fibrin hydrogels. Biomaterials. 2011;32:107-18.

[18] Lambrechts D, Roeffaers M, Goossens K, Hofkens J, Van de Putte T, Schrooten J*, et al.* A causal relation between bioluminescence and oxygen to quantify the cell niche. PLoS One. 2014;9:e97572.

[19] Ignowski JM, Schaffer DV. Kinetic analysis and modeling of firefly luciferase as a quantitative reporter gene in live mammalian cells. Biotechnol Bioeng. 2004;86:827-34.

[20] Thorne N, Auld DS, Inglese J. Apparent activity in high-throughput screening: origins of compound-dependent assay interference. Curr Opin Chem Biol. 2010;14:315-24.

[21] Jonsson P, Jonsson MP, Tegenfeldt JO, Hook F. A method improving the accuracy of fluorescence recovery after photobleaching analysis. Biophys J. 2008;95:5334-48.

[22] Grayson WL, Frohlich M, Yeager K, Bhumiratana S, Chan ME, Cannizzaro C*, et al.* Engineering anatomically shaped human bone grafts. Proc Natl Acad Sci U S A. 2010;107:3299-304.

[23] Leskovac V. Comprehensive enzyme kinetics: Springer; 2003.

[24] Walsh R, Martin E, Darvesh S. A method to describe enzyme-catalyzed reactions by combining steady state and time course enzyme kinetic parameters. Biochim Biophys Acta. 2010;1800:1-5.

[25] Weiner R, Schmitt BA, Podhaisky H. ROWMAP—a ROW-code with Krylov techniques for large stiff ODEs. Appl Num Math. 1997;25:303-19.

[26] Denburg JL, Lee RT, Mcelroy WD. Substrate-binding properties of firefly luciferase .I. Luciferin-binding site. Arch Biochem Biophys. 1969;134:381-94.

[27] Guaccio A, Borselli C, Oliviero O, Netti PA. Oxygen consumption of chondrocytes in agarose and collagen gels: A comparative analysis. Biomaterials. 2008;29:1484-93.

[28] Brown DA, MacLellan WR, Laks H, Dunn JC, Wu BM, Beygui RE. Analysis of oxygen transport in a diffusion-limited model of engineered heart tissue. Biotechnol Bioeng. 2007;97:962-75.

[29] Diepart C, Karroum O, Magat J, Feron O, Verrax J, Calderon PB*, et al.* Arsenic trioxide treatment decreases the oxygen consumption rate of tumor cells and radiosensitizes solid tumors. Cancer Res. 2012;72:482-90.

[30] Jonckheere AI, Huigsloot M, Janssen AJ, Kappen AJ, Smeitink JA, Rodenburg RJ. High-throughput assay to measure oxygen consumption in digitonin-permeabilized cells of patients with mitochondrial disorders. Clin Chem. 2010;56:424-31.

[31] Mohyeldin A, Garzon-Muvdi T, Quinones-Hinojosa A. Oxygen in stem cell biology: a critical component of the stem cell niche. Cell Stem Cell. 2010;7:150-61.

[32] Lambrechts D, Roeffaers M, Kerckhofs G, Roberts SJ, Hofkens J, Van de Putte T*, et al.* Fluorescent oxygen sensitive microbead incorporation for measuring oxygen tension in cell aggregates. Biomaterials. 2013;34:922-9.

[33] Thorpe SD, Nagel T, Carroll SF, Kelly DJ. Modulating gradients in regulatory signals within mesenchymal stem cell seeded hydrogels: a novel strategy to engineer zonal articular cartilage. PLoS One. 2013;8:e60764.
[34] Cidad P, Almeida A, Bolanos JP. Inhibition of mitochondrial respiration by nitric oxide rapidly stimulates cytoprotective GLUT3-mediated glucose uptake through 5'-AMP-activated protein kinase. Biochemical J. 2004;384:629-36.
[35] Fukuda R, Zhang H, Kim JW, Shimoda L, Dang CV, Semenza GL. HIF-1 regulates cytochrome oxidase subunits to optimize efficiency of respiration in hypoxic cells. Cell. 2007;129:111-22.
[36] Pannier AK, Ariazi EA, Bellis AD, Bengali Z, Jordan VC, Shea LD. Bioluminescence imaging for assessment and normalization in transfected cell arrays. Biotechnol Bioeng. 2007;98:486-97.
[37] Zhang Y, Byun Y, Ren YR, Liu JO, Laterra J, Pomper MG. Identification of inhibitors of ABCG2 by a bioluminescence imaging-based high-throughput assay. Cancer Res. 2009;69:5867-75.
[38] Zhang Y, Bressler JP, Neal J, Lal B, Bhang HE, Laterra J*, et al.* ABCG2/BCRP expression modulates D-Luciferin based bioluminescence imaging. Cancer Res. 2007;67:9389-97.
[39] Gandelman O, Allue I, Bowers K, Cobbold P. Cytoplasmic factors that affect the intensity and stability of bioluminescence from firefly luciferase in living mammalian cells. J Biolum Chemilum. 1994;9:363-71.

[40] Fraga H, Fernandes D, Fontes R, da Silva JCGE. Coenzyme A affects firefly luciferase luminescence because it acts as a substrate and not as an allosteric effector. FEBS J. 2005;272:5206-16.

[41] Fraga H. Firefly luminescence: a historical perspective and recent developments. Photochem Photobiol Sci. 2008;7:146-58.

[42] Fontes R, Ortiz B, de Diego A, Sillero A, Gunther Sillero MA. Dehydroluciferyl-AMP is the main intermediate in the luciferin dependent synthesis of Ap4A catalyzed by firefly luciferase. FEBS Lett. 1998;438:190-4.

[43] Gandelman OA, Brovko LY, Chikishev AY, Shkurinov AP, Ugarova NN. Investigation of the interaction between firefly luciferase and oxyluciferin or its analogs by steady-state and subnanosecond time-resolved fluorescence. J Photochem Photobiol B. 1994;22:203-9.

[44] Fraga H, Esteves da Silva JC, Fontes R. pH opposite effects on synthesis of dinucleoside polyphosphates and on oxidation reactions catalyzed by firefly luciferase. FEBS Lett. 2003;543:37-41.

[45] Fontes R, Dukhovich A, Sillero A, Sillero MA. Synthesis of dehydroluciferin by firefly luciferase: effect of dehydroluciferin, coenzyme A and nucleoside triphosphates on the luminescent reaction. Biochem Bioph Res Co. 1997;237:445-50.

[46] Moriyama EH, Niedre MJ, Jarvi MT, Mocanu JD, Moriyama Y, Subarsky P*, et al.* The influence of hypoxia on bioluminescence in luciferase-transfected gliosarcoma tumor cells in vitro. Photochem Photobiol Sci. 2008;7:675-80.

[47] Thompson JF, Hayes LS, Lloyd DB. Modulation of firefly luciferase stability and impact on studies of gene regulation. Gene. 1991;103:171-7.

[48] Keller GA, Gould S, Deluca M, Subramani S. Firefly luciferase is targeted to peroxisomes in mammalian cells. Proc Natl Acad Sci U S A. 1987;84:3264-8.

[49] Sommer JM, Cheng QL, Keller GA, Wang CC. In vivo import of firefly luciferase into the glycosomes of Trypanosoma brucei and mutational analysis of the C-terminal targeting signal. Mol Biol Cell. 1992;3:749-59.

[50] Hulst A, Hens H, Buitelaar R, Tramper J. Determination of the effective diffusion coefficient of oxygen in gel materials in relation to gel concentration. Biotechnol Tech. 1989;3:199-204.

Figures

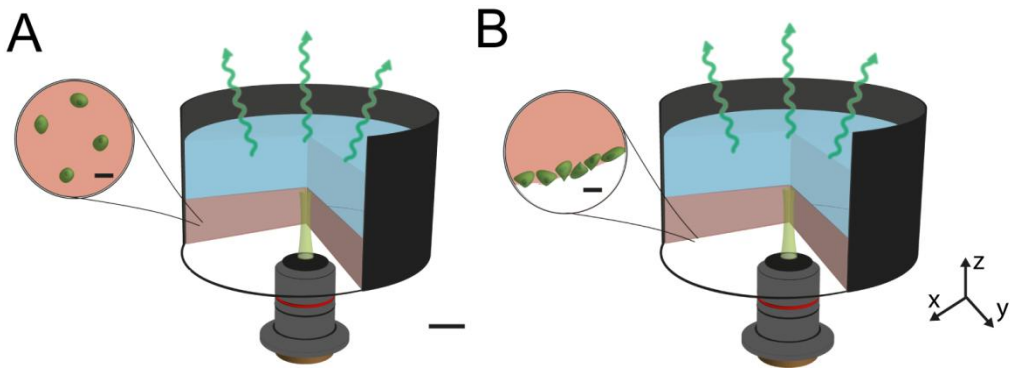

Figure 1

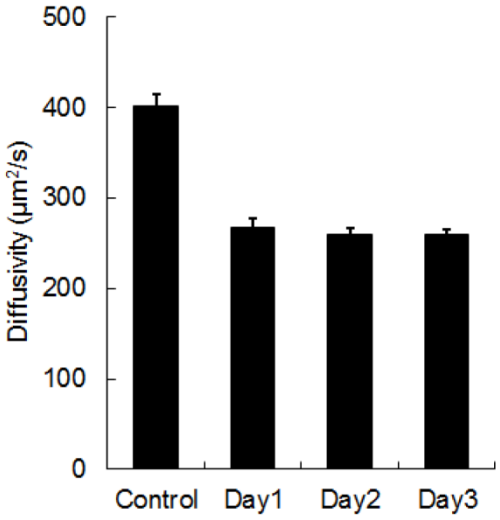

Figure 2

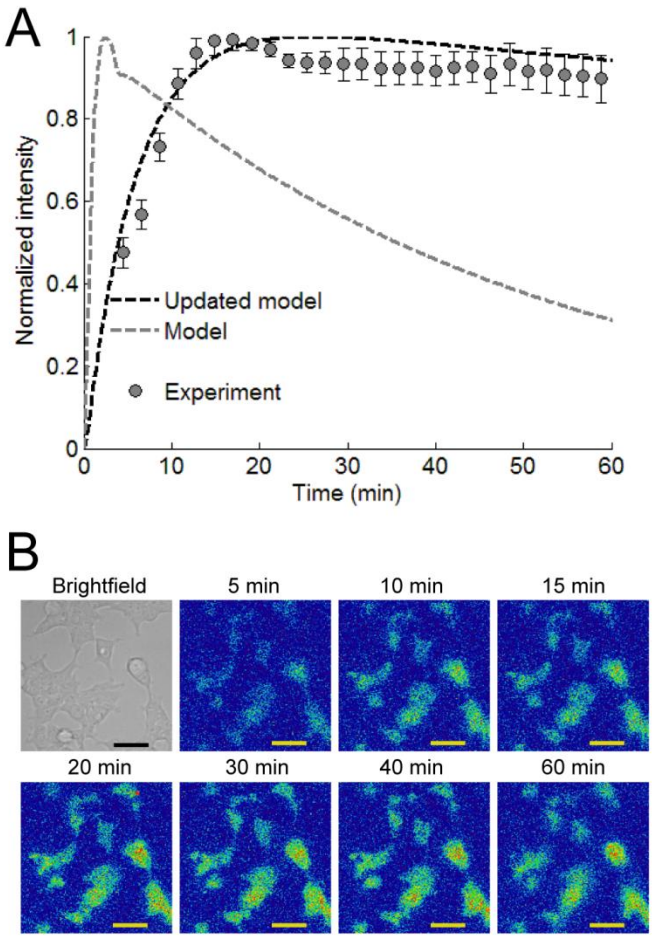
A
Normalized intensity
Time (min)
Updated model
Model
Experiment
B
Brightfield
5 min
10 min
15 min
20 min
30 min
40 min
60 min

Figure 3

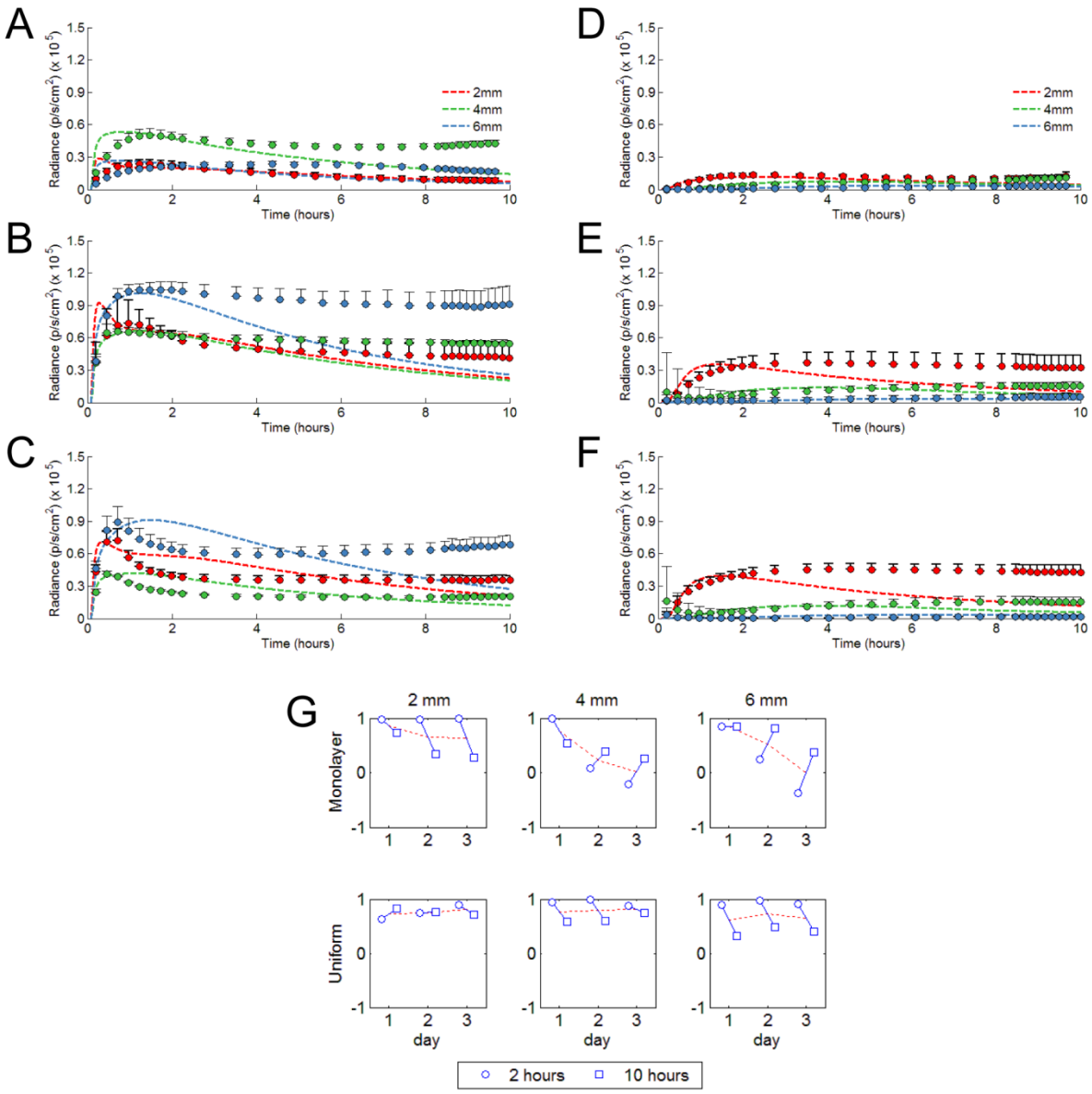
A
B
C
D
E
F
G
Radiance (p/s/cm^2) (x 10^5)
Time (hours)
2mm
4mm
6mm
2 mm
4 mm
6 mm
Monolayer
Uniform
day
2 hours
10 hours

Figure 4

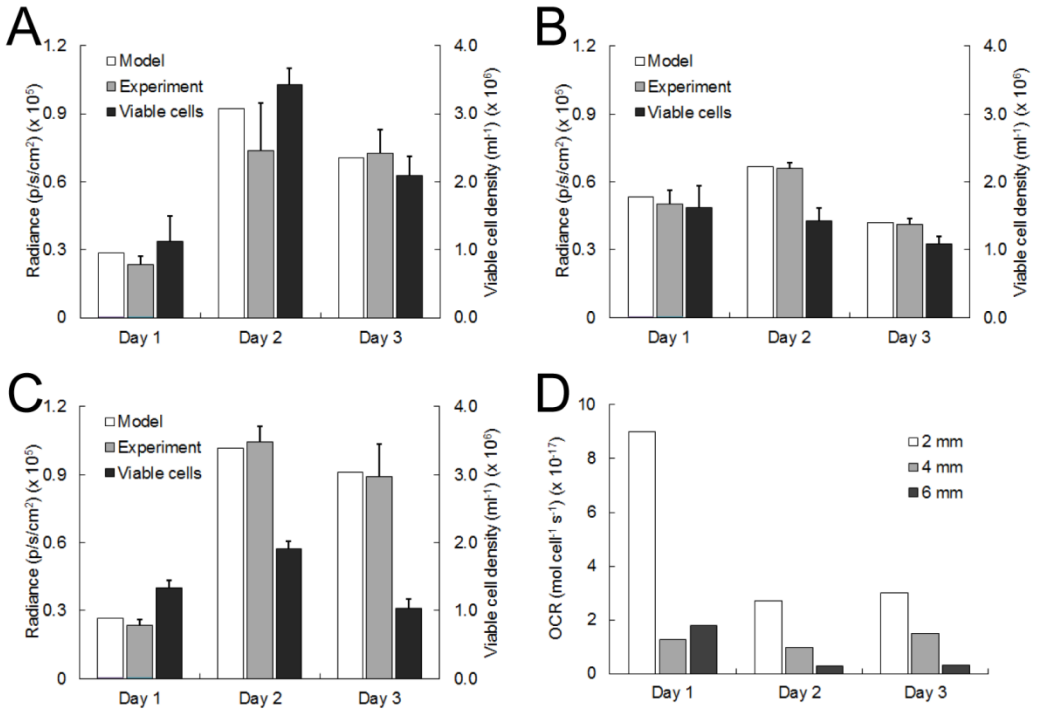

Figure 5

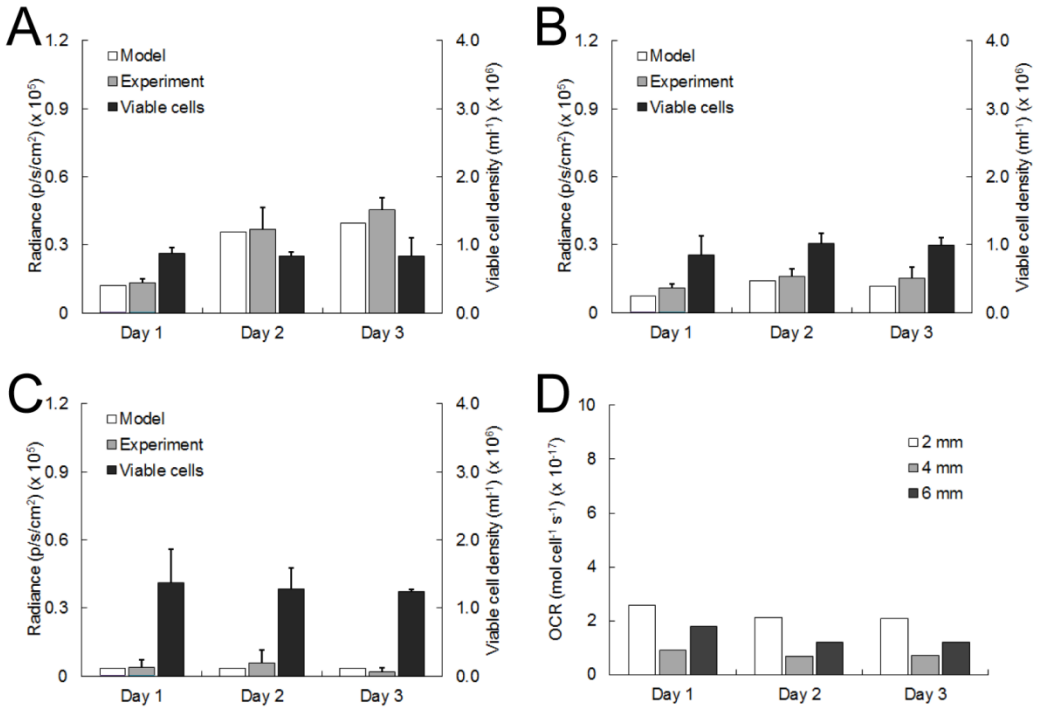

Figure 6

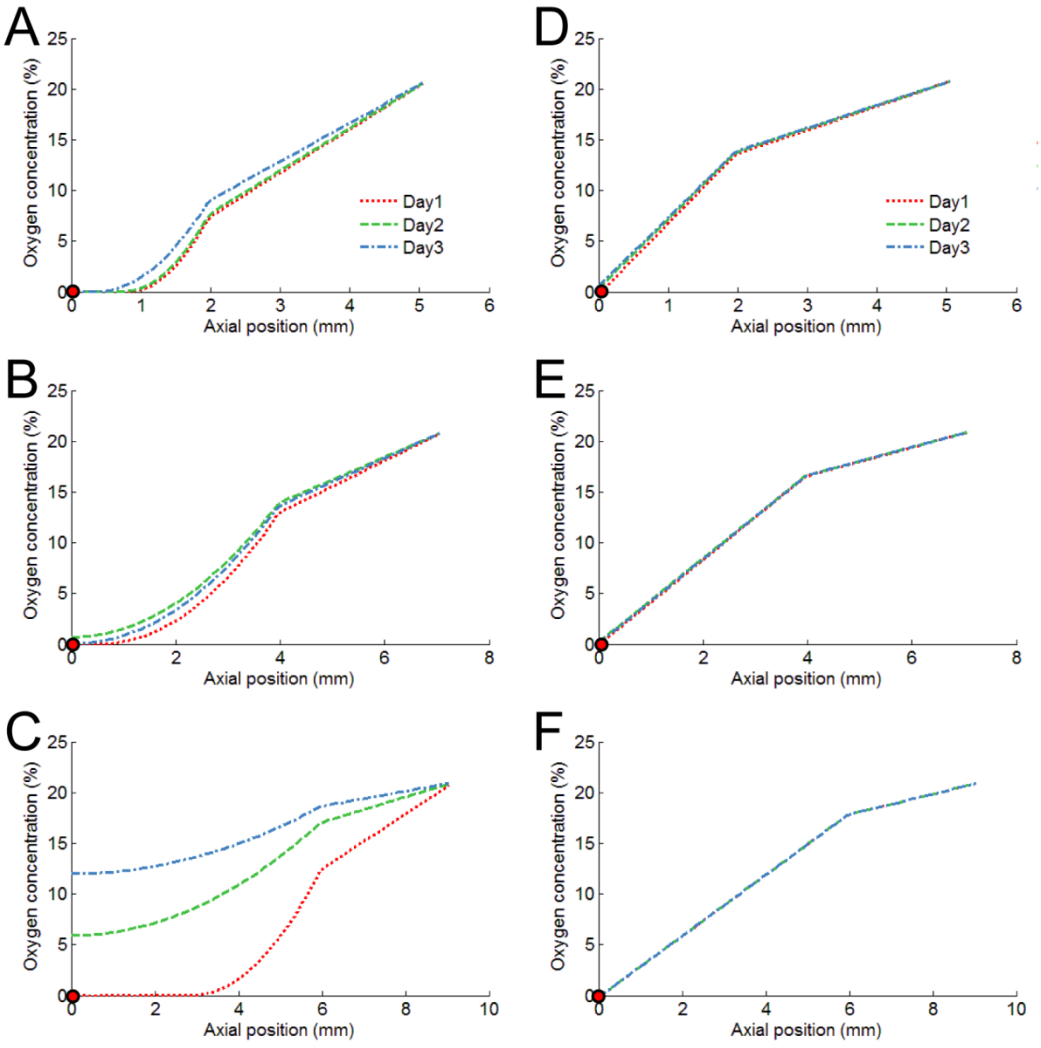
A
B
C
D
E
F
Oxygen concentration (%)
Axial position (mm)
Day1
Day2
Day3

Figure 7

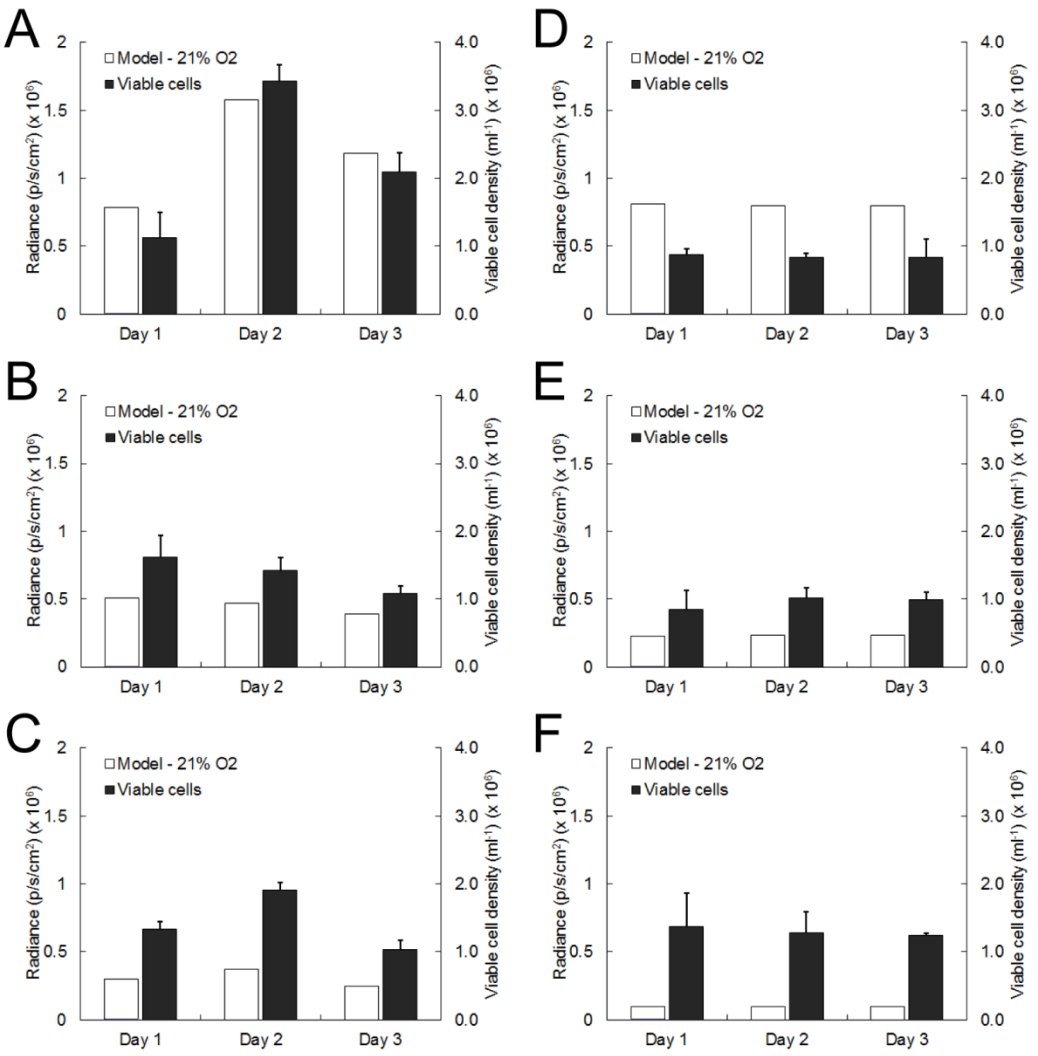
A
B
C
D
E
F
Model - 21% O2
Viable cells
Radiance (p/s/cm²) (x 10⁶)
Viable cell density (ml⁻¹) (x 10⁶)
Day 1
Day 2
Day 3

Figure 8

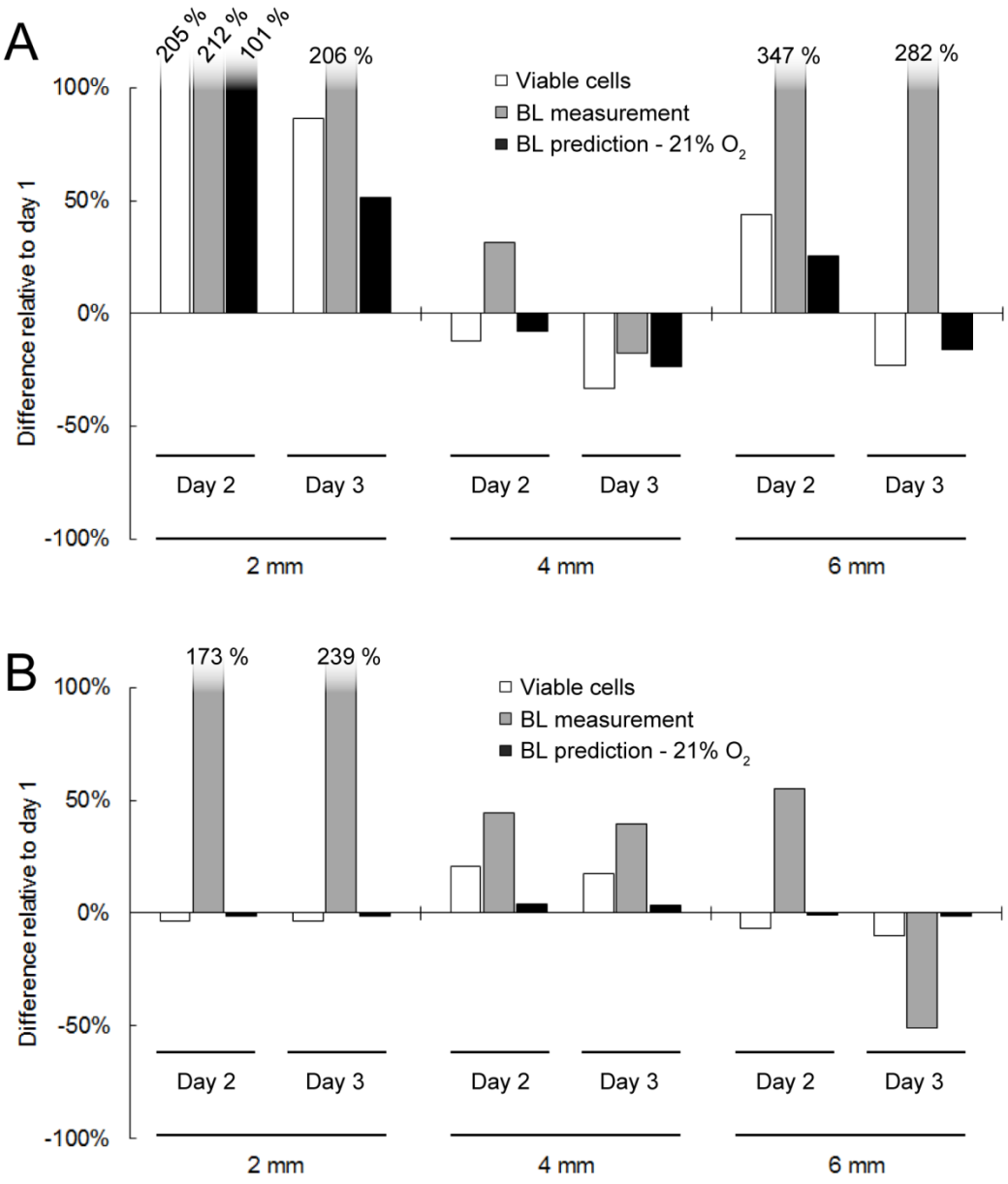
A
205 %
212 %
101 %
206 %
347 %
282 %
Viable cells
BL measurement
BL prediction - 21% O2
Difference relative to day 1
100%
50%
0%
-50%
-100%
Day 2
Day 3
2 mm
4 mm
6 mm
B
173 %
239 %

Figure 9

Model Parameter	Value	Unit	Reference
Luciferin oxidation			
k_{cat} (catalytic rate constant, CRC)	1.1×10^{-4}	mol olc / (mol luc · s) †	Fitted (Fig. 3A)
$k_{cat,21}$ (CRC, 21% O_2)	1.01×10^{-1}	-	
$k_{cat,0}$ (CRC, 0% O_2)	6×10^{-3}	-	
I_{21} (exponential decay constant, 21% O_2)	-2.5	s^{-1}	Fitted (Fig. 3A)
I_0 (exponential decay constant, 0% O_2)	-3	s^{-1}	Measured [18]
$k_{d,Dluc}$ (luciferin decay constant)	4.83×10^{-6}	s^{-1}	Ignowski et al. [19]
Γ (Molecular crowding factor)	1.5	-	Fitted [18]
κ_{21} (transition threshold, 21% O_2)	0.1	-	Fitted [18]
κ_0 (transition threshold, 0% O_2)	15	-	Fitted [18]
Luciferin diffusion			
$D_{Dluc,A}$ (diffusivity in agarose)	9.27×10^{-10}	$m^2\ s^{-1}$	Measured [18]
$D_{Dluc,w}$ (diffusivity in DMEM)	1.00×10^{-9}	$m^2\ s^{-1}$	Measured [18]
$D_{Dluc,m}$ (diffusivity in cell membrane)	1.4×10^{-11}	$m^2\ s^{-1}$	Fitted (Fig. 3A)
λ_m (thickness cell membrane)	4×10^{-9}	m	Ignowski et al. [19]
A_m (Surface area cell membrane)			
for uniform cell distribution:	3.14×10^{-10}	m^2	10 µm sphere
for cell monolayer:	1.57×10^{-10}	m^2	10 µm hemisphere
Luciferase concentration			
$k_{d,luc}$ (luciferase decay constant)	8.33×10^{-5}	s^{-1}	Ignowski et al. [19]

Light production			
RLU	1.38×10^{7}	$p\ s^{-1}\ cm^{-2}$ / (mol olc)	Measured [18]
Oxygen diffusion			
$D_{O2,w}$ (diffusivity in water)	3×10^{-9}	$m^2\ s^{-1}$	Demol et al. [17]
$D_{O2,a}$ (diffusivity in agarose)	1×10^{-9}	$m^2\ s^{-1}$	Hulst et al. [50]

Note: †olc, oxyluciferin complex.

Table 1

Hydrogel dimension	BL measurement	BL prediction - (21% O_2)
Monolayer		
2 mm	-0.9759	0.9999
4 mm	0.9994	0.9998
6 mm	0.2865	0.9998
Uniform distribution		
2 mm	0.8312	0.9955
4 mm	0.4934	0.9995
6 mm	0.3484	0.9989

Table 2

Figure Captions

Figure 1. Illustration of the implemented geometries for the hydrogel screening setup. Luciferase reporter cells (in green) are contained within the agarose hydrogel (in pink) either in a uniformly distributed configuration (**A**) or as a monolayer (**B**). Hydrogels are radially confined by the well borders (in black) of a 96 well plate. At the bottom position, hydrogels are confined by a coverglass base. These geometries depend on passive diffusion from the medium (in blue) that is located on top of the hydrogels as the main transport mechanism for supply of oxygen and luciferin to the reporter cells. Exogenous luciferin is added to this medium at the start of the reporter assay. Scale bar, 1 mm. Scale bar figure insets, 10 µm.

Figure 2. Fluorescein tracer diffusion rates in 2% agarose hydrogels are obtained from FRAP analysis. Measurements of tracer diffusion rate were performed at different time points and compared to an empty (no cells) control hydrogel. No significant time-dependent differences in tracer diffusivity could be observed. Measurements are performed in duplicate with a small shift in spatial position. Error bars, ± 1 s.d. unit; $n \geq 24$.

Figure 3. Decay rates are measured from single cell bioluminescence microscopy. (**A**) Comparison of simulated bioluminescent photon fluxes obtained for luciferase reporter cells incubated with 4.7 µM luciferin. The previous model is based on model parameters that are fitted for reporter cell activity in 470 µM luciferin solutions. The model parameters implemented for the updated model are determined from bioluminescence microscopy of reporter cells exposed to 4.7 µM luciferin. Experimental data for time-dependent luciferase activity is obtained from single cell photon flux measurements. Error bars, ± 1 s.d. unit; $n \geq 8$. (**B**) Bioluminescence microscopy images of 293T reporter cells exposed to saturated (21% O_2) oxygen concentrations (initial luciferin concentration, 4.7 µM). Brightfield image indicates the cell contours. Scale bar, 10 µm.

Figure 4. Simulated (dashes lines) and experimentally measured (dots) bioluminescence reaction dynamics for luciferase reporter cells that were uniformly seeded in a hydrogel (**A-C**) or seeded as a monolayer underneath the hydrogel (**D-F**). Simulation results were obtained using the cell OCR as fitting parameter. Reaction dynamics was measured after 1 (**A**, **D**), 2 (**B**, **E**), or 3 (**C**, **F**) days of static culture and for 3 different hydrogel thicknesses. Dynamic time point measurements were performed during 10 hour periods. Correlation analyses of simulated and experimentally measured bioluminescence data sets were performed for the initial (2 hours) time points and for the total experiment duration (10 hours) (**G**). Correlations were calculated using the Pearson's correlation coefficient. (initial luciferin concentration, 4.7 µM) Error bars, ± 1 s.d. unit; $n = 4$.

Figure 5. Comparison of simulated and experimentally quantified bioluminescence peak intensities for reporter cells uniformly distributed within the hydrogel. Experimental peak intensities are determined from reaction dynamics experiments and the simulated peak intensities result from model fitting. Peak values are measured for three different hydrogel thicknesses of 2 mm (**A**), 4 mm (**B**), and 6 mm (**C**) and are shown together with the experimentally quantified viable cell densities. (**D**) Corresponding values of the cell OCR that were used to fit the model to dynamic time point measurements of the average bioluminescent photon flux. Error bars, ± 1 s.d. unit; *n* = 4.

Figure 6. Comparison of simulated and experimentally quantified bioluminescence peak intensities for reporter cells contained as a monolayer within the hydrogel. Experimental peak intensities are determined from reaction dynamics experiments and the simulated peak intensities result from model fitting. Peak values are measured for three different hydrogel thicknesses of 2 mm (**A**), 4 mm (**B**), and 6 mm (**C**) and are shown together with the experimentally quantified viable cell densities. (**D**) Corresponding values of the cell OCR that were used to fit the model to dynamic time point measurements of the average bioluminescent photon flux. Error bars, ± 1 s.d. unit; *n* = 4.

Figure 7. Oxygen gradients are established within the hydrogel construct. Gradients are predicted from the model using the cell OCRs, which were obtained from fitting the bioluminescent photon fluxes. Results are shown for reporter cells uniformly distributed within the hydrogel (**A-C**) or cells seeded as a monolayer (**D-F**), and for 3 different hydrogel heights of 2 mm (**A**, **D**), 4 mm (**B**, **E**), and 6 mm (**C**, **F**). Red dots indicate the experimentally measured oxygen concentrations using oxygen sensor spots that were located at the hydrogel bottom position.

Figure 8. Oxygen gradient independent bioluminescent peak intensities are simulated for reporter cell activity within uniformly seeded hydrogels (**A**-**C**) or in hydrogels containing a cell monolayer (**D-F**), for a hydrogel thickness of 2 mm (**A**, **D**), 4 mm (**B**, **E**), and 6 mm (**C**, **F**). The peak intensities are obtained by application of a uniform (21% O_2) oxygen concentration within the hydrogel. Peak values are plotted together with the experimentally quantified viable cell densities. Error bars, ± 1 s.d. unit; *n* = 4.

Figure 9. Peak intensities from simulated oxygen-independent reporter cell activity within the hydrogel screening setup are better able to capture the observed changes in viable cell densities as compared to peak intensities from experimentally measured oxygen-dependent reporter cell activity. Relative differences in peak intensities ('BL measurement' and 'BL prediction - 21% O_2') and viable cell density ('viable cells') are shown for hydrogels uniformly seeded with luciferase reporter cells (**A**) or for hydrogels that contain reporter cells in a monolayer (**B**). Differences are given for each hydrogel thickness (2, 4, and 6 mm). The measured

peak intensity and viable cell density obtained after 1 day of static culture were used respectively as a reference for the relative differences given for culture day 2 and 3.

Table 1. Overview of parameter values implemented in the bioluminescence-oxygen model. Most of the parameter values were obtained from the previous model [18], except for the luciferin diffusion coefficient through the cell membrane ($D_{luc,m}$), catalytic rate constant (k_{cat}), and exponential decay constant (I_{21}) which were changed to account for the lower luciferin concentration used in this study. Parameter values that were used in the previous study were 8×10^{-11} $m^2 \cdot s^{-1}$ for $D_{luc,m}$, 1.1×10^{-3} mol olc / (mol luc · s) for k_{cat}, and -27 s^{-1} for I_{21}.

Table 2. Correlation analysis of oxygen-dependent ("BL measurement") and oxygen-independent ("BL prediction - 21% O_2") bioluminescence intensities with the measured viable cell densities for 3 days of static culture.